INTERNATIONAL
Agrophysics
www.international-agrophysics.org

Int. Agrophys., 2026, 40, 143-157
doi: 10.31545/intagr/213588

A novel statistical-physical model of soil heat capacity**

Bogusław Usowicz[1,2], *Jerzy Lipiec*[2]*

[1]Faculty of Civil Engineering and Environmental Sciences, Białystok University of Technology, Wiejska 45 E, 15-351 Białystok, Poland
[2]Institute of Agrophysics, Polish Academy of Sciences, Doświadczalna 4, 20-290 Lublin, Poland

Received August 14, 2025; accepted October 24, 2025

Abstract. The heat capacity is a key parameter affecting heat storage and transfer in soil. Therefore, in this study, we proposed a novel statistical-physical model based on concepts of specific heat, the principle of energy conservation, and configurations of mineral, organic, water, and air particles to estimate the volumetric heat capacity. The novel model does not require the choice of parameters in the equations. It was compared with measured results for soil aggregate beds and two field soils. It can be concluded that the statistical-physical model's predictability of heat capacity was suitable for all the soil specimens. The measured and statistical-physical model-predicted volumetric heat capacities increased with the increasing water content and with the decreasing aggregate size. The good agreement between the model-predicted and measured heat capacities confirmed that the model assumptions regarding the specific heats of soil components and their averaging in the proposed model were adequately established. The proposed easy-to-use and flexible model can be applied to evaluate heat capacity in response to soil management practices and land use. The heat capacities predicted by the statistical-physical model agree well with those from the traditional analytic models proposed by de Vries (1963) and Zhao *et al.* (2016).

Keywords: heat capacity, new model, aggregate beds, field soils, validation

1. INTRODUCTION

The specific heat capacity of soil solids represents the amount of heat required to increase the temperature by one degree for a unit mass of dry soil particles (Kluitenberg, 2002; Wang *et al.*, 2019). Volumetric heat capacity (C_v) is often expressed as the sum of volume fractions of heat capacities of separate soil components, *i.e.*, solid, liquid, and gaseous fractions (de Vries, 1963). The heat capacity of soil is a key parameter that affects heat storage and transfer and determines how rapidly soil can absorb or release heat (Wang *et al.*, 2019).

Soil heat capacity is useful in evaluating heat exchange in green infrastructures of the urban environment (Chun and Guldmann, 2018; Guidolotti *et al.*, 2025) associated with warming due to climate change (Bolinder *et al.*, 2020). One approach includes green roofs with composite soils, including those amended with organic materials, such as biochar and fibre, to improve the hydraulic and thermal properties (Wang *et al.*, 2020) and the cooling capacity of urban green spaces (Guidolotti *et al.*, 2025).

Knowledge of soil heat capacity is an important tool in managing the soil temperature regime for seed germination and crop growth (Noborio *et al.*, 1996; Langa *et al.*, 2024) as well as analysing coupled heat and water transfer in soil (Heitman and Horton, 2011) and frost and heat penetration (Li *et al.*, 2025). Filling the voids during the freezing process with ice, whose volumetric heat capacity is approximately half that of water, results in a noticeable decrease in the volumetric heat capacity of soils (Bi *et al.*, 2024b). Increasing the soil volume heat capacity and thermal conductivity with soil water content makes it easier for the heat of the soil in areas farther away from the pipe and

*Corresponding author e-mail: j.lipiec@ipan.lublin.pl
**This work was partially funded by the HORIZON 2020, European Commission, Programme: H2020-SFS-2015-2: SoilCare for profitable and sustainable crop production in Europe, project No. 677407 (SoilCare, 2016-2021).

containing higher energy to migrate closer to the soil-air heat exchanger and increase the amount of heat stored in the soil, resulting in a slower temperature drop at the same amount of heat released (Jiang and Dong, 2025). The soil thermal parameters constitute crucial information for predicting heat transfer and designing a ground source heat pump system (Tu *et al.*, 2017; Zhang *et al.*, 2024).

The heat capacity is largely affected by several soil factors, such as water content (Kluitenberg, 2002; Zhang *et al.*, 2020), porosity and bulk density (Bi *et al.*, 2024c), soil texture (Bi *et al.*, 2024a), organic matter (Gnatowski *et al.*, 2022) and temperature (Bi *et al.*, 2024a; Lei *et al.*, 2023). Given the linear relationship between the heat capacity and soil water content, Heitman *et al.* (2003) showed that alterations in soil water content ($\Delta\theta$) can be monitored using measurements of the variation in heat capacity (ΔC_v). The field measurement system utilising a dual-probe heat-pulse distributed temperature approach recently developed by Shehata *et al.* (2022) was able to measure the C_v of the soil, from which $\Delta\theta$ was assessed with a high spatial resolution of 0.25 m. The positive relationship between heat capacity and soil water content is influenced by changes in soil bulk density (Lahoori *et al.*, 2020), resulting from soil management and composition. Analysis of heat capacity in compacted soils is important in unsaturated conditions, which predominate in such structures (Lahoori *et al.*, 2020). The impact of bulk density is especially significant in tilled soil and clay soils, where it changes over time due to subsidence as well as shrinking and swelling induced by changes in soil water content (Wang *et al.*, 2023). The range of field soil water content fluctuations is wider in tilled mineral soils than in commonly wetter untilled peat soils (Gnatowski *et al.*, 2022). The above literature indicates that heat capacity not only encompasses knowledge about soil thermal status but also provides information about soil structural indicators, such as bulk density, water content, and associated air content.

Despite the availability of advanced measurement methods, new modelling approaches are needed to forecast soil heat capacity (Shehata *et al.*, 2022). This need is supported by the fact that direct measurement with special instruments by skilled experimental personnel is cumbersome and laborious (Bi *et al.*, 2024a). Furthermore, the need for new models is supported by the increasing interest in studying heat capacity and other thermal properties for better prediction and control of heat transfer and storage (Wang *et al.*, 2019), energy consumption (Luo *et al.*, 2025), seepage velocity (Zhang *et al.*, 2024), and the environment (Luo *et al.*, 2025) in a wide range of soils and spatial scale (Shehata *et al.*, 2022).

Limitations of the existing models include empirical simplifications *e.g.* de Vries' approach treats soil particles as non-contacting uniform ellipsoids (Tarnawski *et al.*, 2021). Therefore, the proposed model considers the volume and shape of cuboid and spherical soil components as thermal capacitors to better predict the soil heat capacity. The model analyses all possible particle configurations of mineral, organic, water, and air particles based on the concepts of specific heat, heat capacity, the principle of energy conservation, and multinomial distribution.

This study aimed to: 1) present and evaluate the novel model with measured results from different soils, and 2) study the effect of soil factors on the novel heat capacity estimation model. The proposed model is an extension of the earlier statistical-physical model of electrical conductivity and permittivity, thermal conductivity, hydraulic conductivity, gas conductivity, and gas diffusivity of substances (Usowicz, 2000).

2. MATERIALS AND METHODS

2.1. Definition and typical values of heat capacity

The heat capacity of soil – C is the amount of heat that must be supplied (or taken away) to the substance/soil for its temperature to increase (or decrease) by 1 K. The unit of heat capacity is J K^{-1}. Specific heat, c, is a thermophysical property that determines the ability of a material to store heat energy and is equal to the amount of heat that must be supplied to a unit mass to cause a unit change in its temperature. The unit of specific heat is J kg^{-1} K^{-1}. The total heat capacity C of a substance is the product of the specific heat c and the mass of the substance m, $C = cm = c\rho V$, where ρ is the density of the substance (kg m^{-3}) and V (m^3) is its volume. The heat capacity can be related to the unit volume V ($C_v = c\rho$ J m^{-3} K^{-1}). Between the specific heat c_i (J kg^{-1} K^{-1}) of individual soil components and their heat capacity per unit volume C_{vi}, there is a dependence: $C_{vi} = c_i\rho_i$, where ρ_i (kg m^{-3}) – the density of soil components.

The volumetric heat capacity of soil C_v depends on the heat capacity per unit volume of individual components of the solid phase (particles of various minerals and organic matter), the liquid phase (free and bound water), ice, the gas phase (soil air), and the proportions of these components in the soil:

$$C_v = \sum_{i=1}^{n} x_{si} C_{si} + x_w C_w + x_a C_a, \qquad (1)$$

where: x_{si}, x_w, x_a (m^3 m^{-3}) – the share of components in a unit volume of the solid, liquid, and gaseous phase, C_{si}, C_w, C_a (J m^{-3} K^{-1}) – the heat capacity per unit volume of the components of the solid, liquid, and gaseous phase.

The measurements showed that the average density of mineral components of the soil solid phase is about 2.65 Mg m^{-3}, and their heat capacity per unit volume C_s is equal to 2.0 MJ m^{-3} K^{-1}. The density of organic matter in the soil is about 1.3 Mg m^{-3}, and its C_o is about 2.5 MJ m^{-3} K^{-1}. The density of water is more than twice that of minerals, but C_w is more than twice that of C_s and is about 4.2 MJ m^{-3} K^{-1}. The density of air is equal to about 1/1 000 of that of water,

and its C_a is equal to 1.25 kJ m^{-3} K^{-1}. As can be seen, it does not contribute much to the overall C_v and is often omitted in calculations.

The research shows that, for typical soils, the variability of the solid content ranges from 0.45 to 0.65 m^3 m^{-3}, and the heat capacity per unit volume C_v varies from about 1 MJ m^{-3} K^{-1} in the air-dry state to over 3 MJ m^{-3} K^{-1} in the state of full water saturation. With the unchanging content of mineral and organic components, the heat capacity – C_v depends only on soil moisture, and it is an almost linear relationship in the entire range of moisture variability. Some nonlinearity is observed for the soil at very low water content. Soil density and soil structure have less effect on heat capacity than water content. The value of heat capacity increases as the density increases. To calculate the value of heat capacity per unit volume – C_v (MJ m^{-3} K^{-1}), the empirical formula given by de Vries (1963) is often used:

$$C_v = (2.0x_s + 2.51x_o + 4.19x_w)10^6, \quad (2)$$

where: x_s, x_o, x_w (m^3 m^{-3}) – the share of mineral and organic parts and water in the unit volume of soil.

2.2. Novel statistical-physical model of heat capacity

The novel statistical-physical model of heat capacity considers specific heat and density of both mineral and organic components, gas and liquid, temperature, pressure, and their variations depending on the medium's state. This model is an extension of earlier statistical-physical models of electrical conductivity and permittivity, thermal conductivity, hydraulic conductivity, gas conductivity, and diffusivity of gas and substance (Usowicz, 2000). The statistical-physical model of the soil heat capacity was based on the concepts of specific heat, heat capacity, the principle of energy conservation, and multinomial distribution. The capacitance of a thermal capacitor depends on the type of medium and the volume/shape. Cuboid and spherical thermal capacitors were considered (Fig. 1). It is assumed that the heat capacity of a material/substance is isotropic, *i.e.*, is the same in all directions in contrast to thermal conductivity, which can be highly anisotropic.

The heat capacity of a cuboid-shaped capacitor C_{cs} is equal to $C_{cs} = c\rho V = c\rho Al$, while that of a spherical-shaped Css condenser is $Css = c\rho V = \frac{4}{3}\pi c\rho r^3$, where: V – volume (m^3), c – specific heat (J kg^{-1} K^{-1}), ρ – density (kg m^{-3}), A – area (m^2), l – length (m), r (m) – the radius of the sphere. The heat capacities of the condensers of spherical soil particles are expressed in formulas depending on the main components of the soil: quartz capacity: $Cq = c_q\rho_q V_q = \frac{4}{3}\pi c_q\rho_q r_{ij}^3$, other minerals: $C_{mi} = c_{mi}\ \rho_{mi}\ V_{mi} = \frac{4}{3}\pi c_{mi}\rho_{mi} r_{ij}^3$, organic matter: $C_o = c_o\ \rho_o\ V_o = \frac{4}{3}\pi c_o\rho_o r_{ij}^3$, water: $C_l = c_l\ \rho_l\ V_l = \frac{4}{3}\pi c_l\rho_l r_{ij}^3$, ice: $C_i = c_i\ \rho_i\ V_i = \frac{4}{3}\pi c_i\rho_i r_{ij}^3$, and air/gases: $C_a = c_a\ \rho_a\ V_a = \frac{4}{3}\pi c_a\rho_a r_{ij}^3$, where: r_{ij} (m) – radius of the i-th sphere in layer and in the j-th layer.

It is assumed that in the layer in the cuboid, there are u thermal capacitors and there are n such layers. The resultant heat capacity C_{cs} of the entire system was calculated by adding up the capacitances of capacitors in the layer and in the layers (Fig. 1). The heat capacity of the layer is:

$$C_j = \sum_{i=1}^{u} C_{ij}. \quad (3)$$

The heat capacity of the connected layers is equal to the sum of all the layers:

$$C_{cs} = \sum_{j=1}^{n} C_j = \sum_{j=1}^{n}\sum_{i=1}^{u} C_{ij}. \quad (4)$$

Let the layer in the cuboid with area A correspond to u unit surfaces (m^2), and the layers with length l correspond to n unit lengths (m). The heat capacity of a cuboid with u and n layers was calculated using the formula: $C_{cs} = c\rho V = c\rho un$. Soil consists of solid, liquid, and gaseous particles with $k = 1, ..., l$ soil components. Substituting $C_{ij} = \frac{4}{3}\pi c_k\rho_k r_{ij}^3$ into the equation for the total heat capacity C_{cs}, taking into account l components of the soil and dividing by un, we get the heat capacity per unit volume C_v (J m^{-3} K^{-1}):

$$C_{cs} = c\rho un = \frac{4\pi}{3}\sum_{j=1}^{n}\sum_{i=1}^{u}\sum_{k=1}^{l} c_k\rho_k r_{ij}^3. \quad (5)$$

Dividing the volume of a sphere with radius r_{ij} by a unit volume can be considered as scaling the volume of the sphere to a unit volume. It is assumed that all the radii of spheres are equal. Dividing the volume of the sphere $\frac{4}{3}\pi r_{ij}^3$

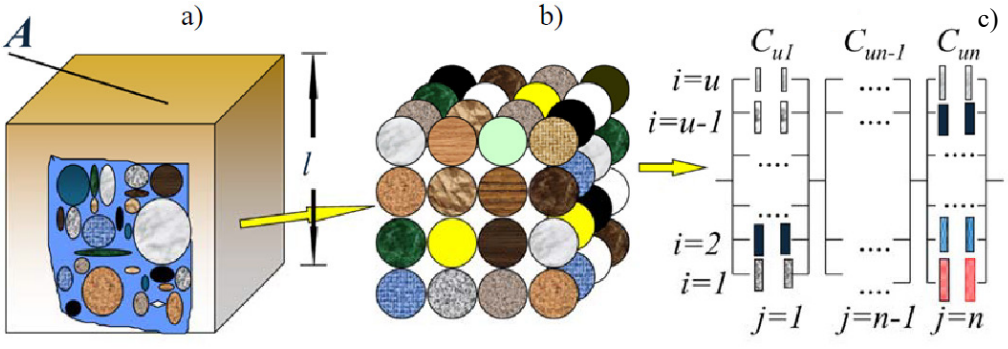

Fig. 1. Schematic diagram of the structure of the statistical-physical heat capacity model where: a) unitary volume of soil, b) the system of spheres that forms n layers, c) representation of contacts in layers by u parallel connection of heat capacitors.

by n unit lengths will reduce the volume of the sphere to the area of the sphere $4\pi r_{ij}^2$ with the factor (value of rescaling) of the reduction as an equivalent radius r_k (-). Dividing the surface of the sphere by the u area (r_{ij}^2) equal to the base of the cuboid with side r_{ij}, we get the value:

$$C_v = c\rho = \frac{4\pi r_k}{un}\sum_{j=1}^{n}\sum_{i=1}^{u}\sum_{k=1}^{l} c_k\rho_k. \quad (6)$$

By substitution:

$$a_j = \sum_{i=1}^{u}\sum_{k=1}^{l} c_k\rho_k, \quad (7)$$

and from the definition of the average value for:

$$\overline{a}(c_k,\rho_k) = \frac{1}{n}\sum_{j=1}^{n} a_j. \quad (8)$$

A general formula for the average value of the heat capacity of a capacitor consisting of various substances with specific heat c_k and density ρ_k is obtained:

$$C_v = \frac{4\pi r_k}{u}\overline{a}(c_k,\rho_k). \quad (9)$$

The medium can be considered as a finite number of soil component particles, where the density and specific heat of the components may depend on the temperature $\rho_k(T)$, $c_k(T)$. In a unit volume of medium/soil, one can find x_1 particles of the first component with specific heat c_1 and particle density ρ_1, x_2 particles of the second component with c_2 and ρ_2, *etc*., with the total number of particles being $x_1 + x_2 + \ldots + x_k = u$. Substituting $\rho_k(T)$ for ρ_k, and $c_k(T)$ for c_k, the expression for a_j is written as follows:

$$a_j = x_{1j}\rho_1(T)c_1(T) + x_{2j}\rho_2(T)c_2(T) + \cdots + x_{kj}\rho_k(T)c_k(T). \quad (10)$$

In the medium/soil with a constant mineralogical composition, the value will depend on the water content in the unit volume of soil – θ_v, total porosity – φ, specific heat of individual components of the medium – c_i, temperature – T, density of soil particles – ρ_i, number of individual particles – x_i, and the number of parallel connections between soil particles treated as heat capacities – u. Thus, the heat capacity can be expressed by:

$$C_v = \frac{4\pi r_k}{u}\bar{a}(\theta_v,\phi,\rho_k,c_k,T,x_i). \quad (11)$$

Since it is impossible to find the distribution of particles in the soil experimentally, and thus the mean value – $\bar{a}(\theta_v, \phi, \rho_k, c_k, T, x_i)$, the mean value can be replaced with the expected theoretical value – $\overline{m}(\theta_v, \phi, \rho_k, c_k, T, x_i)$, which takes into account all possible particle configurations and the probabilities of these configurations:

$$C_v = \frac{4\pi r_k}{u}\bar{m}(\theta_v,\phi,\rho_k,c_k,T,x_i). \quad (12)$$

On the other hand, the expected value was calculated in accordance with the definition from the formula:

$$\bar{m} = \sum_{j=1}^{L} a_j P(X = x_j), \quad (13)$$

where: $P(X = x_j)$ is the probability (realisation of the random variable $P(X = x_i)$, X taking numerical values equal to $x_1,\ldots,x_L$), whereby: $\sum_{i=1}^{k}$, $x_{ij}=u$, $j=1.2,\ldots, L$, $P(x_{ij})$ – the probability of a given configuration of soil particles. The following condition must also be met: $\sum_{j=1}^{L} P(X=x_j) =1$. Taking into account all possible configurations of combined heat capacitors, the general formula for the volumetric heat capacity of the medium/soil was obtained:

$$C_v = \frac{4\pi r_k}{u}\sum_{j=1}^{L}(x_{1j}\rho_1(T)c_1(T)+\ldots+x_{kj}\rho_k(T)c_k(T))P(x_{1j},\ldots,x_{kj}). \quad (14)$$

The probability of the occurrence of a given configuration of heat capacitors $P(x_{1j}, \ldots, x_{6j})$ in the physico-statistical model of heat capacity was calculated from the multinomial distribution with six main components of soil k, *i.e*. quartz q, other minerals m, organic matter o, water w, ice i, and air a, with the content of soil components f_i in unit volume and the number of heat capacitors x_k:

$$P(x_q,x_m,x_o,x_w,x_i,x_a) = \frac{u!}{x_q^!x_m^!x_o^!x_w^!x_i^!x_a^!} f_q^{x_q} f_m^{x_m} f_o^{x_o} f_w^{x_w} f_i^{x_i} f_a^{x_a}. \quad (15)$$

Considering the fact that the heat capacity of the air (1 295 J m^{-3} K^{-1}) is very small in relation to other soil components, it is often omitted in calculations. Then, the probability is reduced to five elements:

$$P(x_q,x_m,x_o,x_w,x_i) = \frac{u!}{x_q^!x_m^!x_o^!x_w^!x_i^!} f_q^{x_q} f_m^{x_m} f_o^{x_o} f_w^{x_w} f_i^{x_i}. \quad (16)$$

In water-unsaturated soil and a large temperature gradient, there is a flow in the way of water vapour, which is characterised by a significant heat capacity C_v = 1 149.7 kJ m^{-3} K^{-1}. The heat capacity of water vapour can be considered in the gas phase with known water vapour content in the soil. The specific heat, *i.e*., the amount of heat needed to raise the temperature of a given substance in a known form by one degree Celsius, is 4.187 kJ kg^{-1} K^{-1} for water, 2.108 kJ kg^{-1} K^{-1} for ice, and 1.996 kJ kg^{-1} K^{-1} for water vapour. The density of water is ~1 000 kg m^{-3}. The density of water vapour at 100°C and 1 atm pressure is ~0.6 kg m^{-3} (5.98 × 10^{-4} g cm^{-3}).

The apparent heat capacity C_a takes into account the latent heat of melting/freezing (when water freezes, it gives off heat, and when it thaws, it takes heat in the same amount as it gives off):

$$C_{va} = C_v + L_f\rho_l\frac{\partial\theta_l}{\partial T} = C_v + L_f\frac{\partial w}{\partial T}, \quad (17)$$

where: w is the change in the total volume of ice and liquid water (COMSOL, 2023):

$$w = \frac{1}{2}\frac{\theta_l\rho_l - \theta_i\rho_i - \rho_b}{\theta_i\rho_i + \theta_l\rho_l + \rho_b}. \quad (18)$$

The apparent heat capacity can be explained as the amount of energy required to raise the temperature per unit volume of partially frozen soil by one degree, even when there is a phase change between liquid water and ice due to temperature change, L_f is the latent heat of melting, 3.34 ×

10^5 J kg^{-1}, C_{va} – total heat capacity of soil with latent heat, ρ_l – density of water, ρ_i – density of ice, ρ_b – density of soil, θ_l – water content, θ_i – ice content, and T – temperature.

2.3. Parameters of the statistical-physical model of heat capacity

In the earlier statistical-physical model relating to thermal conductivity, the radius of the spheres as well as the number of parallel connections of the spheres changed, depending on the content of the dominant soil component and soil water saturation. The radius of the spheres of r_k varied from 0.044 to 0.08, depending on the dominant component in the soil. With a mixture of components, the radius was the smallest, and with one folding, it was the largest. The number of parallel joints of the spheres varied from 3 to 13, depending on the degree of water saturation of the soil. In contrast, in the dielectric permittivity model, the radius of the spheres was constant and amounted to 0.08. At this value, the model scales to the dielectric permittivity (dielectric constant) that a given component can achieve at 100% of the content, *e.g.*, if it is water, it will be approximately 80 (78.4) at a temperature of 25°C. If it were the heat capacity, it would be equal to 4 161 090 J m^{-3} K^{-1} (specific heat of water 4 182 J kg^{-1} K^{-1}). In the statistical-physical model of heat capacity, it was assumed that the number of parallel connections of spheres varies from 3 to 13, depending on the degree of soil water saturation, similar to the thermal conductivity of soil. As water saturation increases, thermal bridges form around the solids, and the conductivity and capacity increase.

The number of parallel connections of thermal capacitors "u" as a function of soil water saturation ($\theta v/\phi$) is shown in Fig. 2. It was assumed that the particles of the solid, liquid, and gaseous phases would be represented by the same equivalent radius of spheres $r_k = 0.08$.

A step transition of the "u" value as a function of soil water saturation also causes a step increase in the calculated values of soil heat capacity. Similar to thermal conductivity, a procedure for the indirect determination of heat capacity within a given soil saturation interval has been proposed. The method consisted in determining the heat capacity of the soil from the statistical-physical model from the formula (C_v) for two successive values of u and u+1 (Fig. 2) and corresponding to the water contents $\theta_v(u)$, $\theta_v(u+1)$, and then the value of the heat capacity for the searched water content was determined from the linear equation given below:

$$C_v = C_v(u) + \frac{C_v(u+1) - C_v(u)}{\theta(u+1) - \theta(u)}\left(\theta_v - \theta_v(u)\right). \quad (19)$$

The statistical and physical model takes into account the basic physical and thermal properties of the main components of the soil and the volumetric content of the solid, liquid, and gaseous fractions of the soil, which are related to the unit volume of soil. The relative soil components to the unit volume of soil are regarded as the probability of drawing a specific particle of the solid, liquid, and gaseous phases of the soil in a single sample. The contents of individual mineralogical components in the soil can be derived from known measured data or can be estimated from soil granulometric compositions. The main mineralogical components of the soil are taken into account, *i.e.*, quartz, other minerals, organic matter with biochar, water and air and their specific heats, densities, and changes induced by temperature and pressure. The total porosity of the soil φ was calculated from the equation: $\phi = 1 - \frac{\rho_b}{\rho_s}$. It equaled the air content $\phi = f_g$, in the soil when there was no water. When there was water, the air content in the soil decreases by this part of the water/ice, according to the equation: $fg = 1 - \left(\frac{\rho_b}{\rho_s} + \theta_l + \theta_i\right)$. It was assumed approximately that the general porosity ϕ of the soil is equal to the water content in the soil in the state of full saturation of the soil with water θ_s, $\phi = \theta_s$. The air content was calculated from the equation:

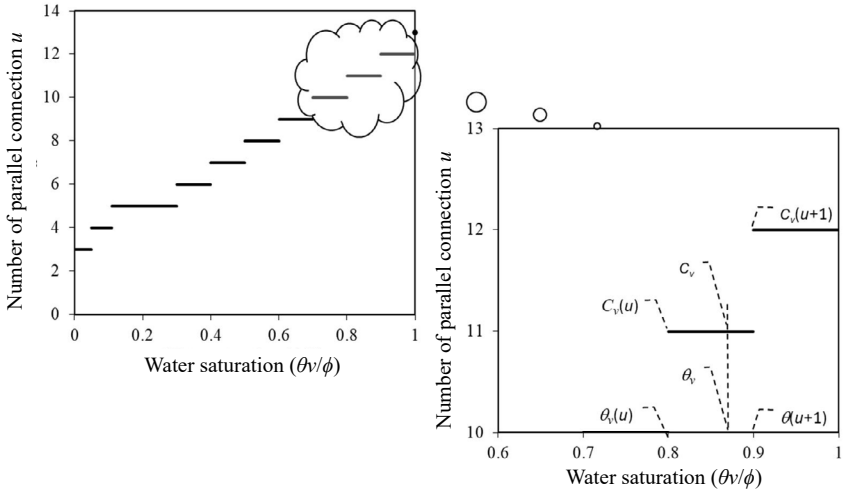

Fig. 2. Number of parallel connections "u" as a function of soil saturation with water $\theta v/\phi$.

$f_g = \theta_s - (\theta_l + \theta_i)$. If the measurements showed the water content in the fully saturated state and the density of the solid phase of the soil, then the soil density can be estimated as follows: $\rho_b = \rho_s (1-\phi)$, or $\rho_b = \rho_s (1-\theta_s)$.

2.3.1. Thermal properties and densities of the main soil components of the solid, liquid, and gaseous phases – estimates and calculations

The heat capacity per unit volume was calculated taking into account the following components: quartz, other minerals, organic matter with biochar, water content in soil, and air. The specific heat capacity of quartz (J kg^{-1} K^{-1}) for the particle density ρ_s = 2 654 kg m^{-3} as a function of temperature was calculated from the equation proposed by Kekelia (2012):

$$c_{p\_quartz} = 2.8743\times10^{-6} T^3 - 3.1599\times10^{-3} T^{-2} + 1.8762 T + 696.54. \quad (20)$$

The specific heat capacity variation of water with temperature is not very large (approximately 1% within the 0-50°C range). Water specific heat capacity c_p (kJ kg^{-1} K^{-1}) variation with temperature (Kekelia, 2012):

$$c_{p\_water} = 9.8933\times10^{-9} T^4 - 1.5591\times10^{-6} T^3 + 1.0407\times10^{-4} T^2 - 3.2972\times10^{-3} T + 4.2192. \quad (21)$$

Water density ρ_w (kg m^{-3}) variation with temperature:

$$\rho_w = -3.4671\times10^{-7} T^4 + 6.7777\times10^{-5} T^3 - 8.5411\times10^{-3} T^2 + 6.4701 T + 999.85. \quad (22)$$

Ice specific heat capacity variation with temperature: c_{p_ice} (J kg^{-1} K^{-1}) (Kekelia, 2012):

$$c_{p\_ice} = 1.3642\times10^{-5} T^3 + 5.4463\times10^{-3} T^2 + 7.5938 T + 2098.8. \quad (23)$$

Ice density variation with temperature: ρ_{ice} (kg m^{-3}):

$$\rho_{ice} = 7.6944\times10^{-7} T^3 - 1.7506\times10^{-4} T^2 - 1.46\times10^{-1} T + 916.73. \quad (24)$$

Zografos *et al.* (1987) provide polynomials to compute specific heat at constant pressure of air as a function of static temperature T_s on the Kelvin scale as follows:

Specific heat of air at constant pressure (c_{p_air}) variation with temperature in units of J kg^{-1} K^{-1}:

$$c_{p\_air} = 1.3864\times10^{-10} T^4 - 6.47474\times10^{-7} T^3 + 1.02344\times10^{-3} T^2 - 0.432819 T + 1061.332. \quad (25)$$

Air density (ρ) in units of kg m^{-3}: $\rho = P_s / R T_s$, where P_s is the static pressure in Pascal, and the gas constant has the value R = 287.058 J kg^{-1} K^{-1}, T_s temperature in K. Since the dry air density can be calculated as $\rho = P_s/(R \times T_s)$ with R = 287.058 J kg^{-1} K^{-1}, at 101 325 Pa and 20°C = 293.15 K, we get: ρ = 101 325 / (287.058 × 293.15) = 1.204 kg m^{-3}.

The specific heats entering other c_{im} minerals can be derived from measurements or be estimated as geometric means from the knowledge of the dominant components. The equivalent heat capacity of the two components was calculated from the equation: $c_{im} = c_m^{f_m} c_j^{1-f_m}$, where c_m and c_j are the specific heats of the minerals and f_m is the volumetric content of the mineral m. With more components of other soil minerals, the geometric mean can be calculated from the general equations: $c_{im} = \prod_j c_{mj}^{f_j}$, and $\sum_j f_j = 1$, where c_{mj} is the specific heat capacity of soil component (mineral) j; f_j is the volumetric fraction of soil component (mineral) j. Specific heats of selected clay minerals at 300 K and their densities, which enter mainly into other minerals in the model: illite (0.962 kJ kg^{-1} K^{-1}), Na-kaolinite (0.931 kJ kg^{-1} K^{-1}), and Ca-kaolinite (0.811 kJ kg^{-1} K^{-1}), with densities of 2.6 Mg m^{-3}, Na (0.779 kJ kg^{-1} K^{-1}), and Ca (0.808 kJ kg^{-1} K^{-1}) – montmorillonite with densities of 2.4 Mg m^{-3} and Attapulgite (0.742 kJ kg^{-1} K^{-1}) with densities of 2.2 Mg m^{-3} (Skauge *et al.*, 1983). The specific heat of other minerals (silt and clay fractions) without knowing the mineralogical composition was estimated from an experiment (Clauser, 2021): density, specific heat, and volumetric heat capacity of the selected minerals at 20°C, ρ_{clay} = 2.68 Mg m^{-3}, c_p = 0.86 kJ kg^{-1} K^{-1}, C_v = 2.300 MJ m^{-3} K^{-1}. In the de Vries model (de Vries, 1963), the specific heat of the mineral c_m and the specific heat of organic matter were assumed as 0.725 and 1.92 MJ Mg^{-1} K^{-1}, respectively. The particle density of organic matter was 1.3 Mg m^{-3}.

2.4. Measuring the specific heat of soil aggregate beds

The specific heat of soil aggregates was determined experimentally with the calorimetric method (Sikora, 1983). The specific heat of the solid phase of wet soil samples was measured to ignore the heat of wetting. It has been shown that the heat of wetting can be omitted when the water content of soil samples is higher than the double hygroscopic maximum water capacity (Sikora and Malicki, 1984). The calorimeter built by Sikora (1983) consisted of two vessels. A vessel in the shape of an aluminium cylinder, 0.3 mm thick, 40 mm radius, and 90 mm high, was placed in a Dewar thermos. The dishes and lids were properly insulated. Temperature measurements in the calorimeter were carried out with copper-constantan thermocouples. Soil samples with mass m and water content θ were heated to the temperature T_1 (approx. 25°C). Distilled water weighing m_w and at a temperature of about 5°C was poured into the inner vessel of the calorimeter. The space between the vessels of the calorimeter was cooled with nitrogen vapour, which prevents water from heating up from the environment. As a result of heat transfer, the state of thermal equilibrium T_2 was established. This state was identified on the basis of changes in the temperature of distilled water in the calorimeter from the moment of introduction of nitrogen vapours between the calorimetric vessels. When the temperature of distilled water was set at T_2, a soil sample was placed in the calorimeter after its initial temperature T_1 had been measured. The soil sample was quickly mixed with distilled water. As a result of heat transfer, the equilibrium temperature of T_3 was established. As a result of the experiment, the temperature changes of

the soil sample were $T_1 - T_3$ and water $T_3 - T_2$, respectively, which allowed solving the heat balance equation from the formula (Sikora, 1983):

$$c\, m(T_1 - T_3) = (c_w\, m_w + A)\,(T_3 - T_2). \quad (26)$$

The specific heat c of the moist soil sample was calculated from the equation:

$$c = \frac{(c_w m_w + A)(T_3 - T_2)}{m(T_1 - T_3)}, \quad (27)$$

where: A – heat capacity of the inner vessel of the calorimeter (A = 29 J K^{-1}), c_w – specific heat of distilled water (c_w = 4 190 J kg^{-1} K^{-1}). For example, the specific heat c of a moist soil sample with a mass of m = 0.06 kg, a water content of θ = 0.35 kg kg^{-1}, and a water mass m_w = 0.05 kg was calculated, with a change in the temperatures of the soil sample and distilled water of 12 and 5°C, respectively (Sikora, 1983). After substitution, the following were obtained:

$$c = \frac{(4190x0.05+29)5}{0.06x12} = 1656.25 \text{ J kg}^{-1} \text{ K}^{-1}. \quad (28)$$

The specific heat of the solid phase of the soil was calculated from the equation: $c_s = c(1+\theta) - c_w\,\theta$ based on the specific heat of the soil sample: $c = \frac{c_s + c_w\theta}{1+\theta}$ with water content θ expressed in kg kg^{-1} (Sikora, 1983). Substituting the above data into the equation, the following data were obtained: c_s = 1 656.25 (1 + 0.35) - 4 190×0.35=769.43 J kg^{-1} K^{-1}.

The volumetric heat capacity of the aggregates as a function of water content θ (m^3 m^{-3}) in the soil was calculated from a linear equation taking into account the measured soil densities ρ (kg m^{-3}) and specific heat of the solid phase of individual fractions of soil aggregates cs and water (4 190 J kg^{-1} K^{-1}):

$$C_v = c_s\,\rho + 4190\,\theta. \quad (29)$$

The heat capacities calculated from the specific heat of aggregates, soil density, and water content in the soil (Sikora, 1983) were compared with those calculated from statistical-physical and de Vries heat capacity models. The statistical-physical model used the granulometric composition of the soil as input to estimate the content of quartz and other minerals, the content of organic matter, the amount of biochar added, the density of the solid phase of the soil, the density of the soil, and the water content and temperature of the soil. The specific heat of soil components, depending on temperature, density, and pressure, was used in the model for quartz, water, and air. Constant values of specific heat and, in some cases, geometric averages taking into account the content of nutrients in the soil, were used for the other soil components. The specific heat and density of organic matter and biochar, if known, were averaged as the geometric mean. In the case of organic matter and biochar, if they were not known, the data estimated by de Vries were used, and the biochar data from the available literature for similar components and temperatures were used.

2.5. Data collection

2.5.1. Soil aggregate beds

Soil samples were collected from Haplic Phaeozem (WRB, 2015) located in Werbkowice, SE Poland (50°45' N, 23°41' E). As to textural class, the soil was referred to as a silty loam (Lipiec *et al.*, 2007). After drying in the laboratory to an air-dry state, the soil was sieved through a set of sieves (with mesh sizes of 10, 5, 3, 1, 0.5, and 0.25 mm) to make beds with fractions <0.25, 0.25-0.5, 0.5-1, 1-3, 3-5, and 5-10 mm. The specific heat of mono-aggregate beds was measured for 9 selected water contents within the entire range of water contents, obtained at different tensions, and additionally by drying at room temperature (20°C). The soil properties listed in Table 1 were used to estimate the heat capacity of soil aggregates using a statistical-physical model of heat capacity.

Table 1. Characteristics of the Haplic Phaeozem in Werbkowice, Poland*

Aggregate size (mm)	Particle size (mm) distribution (%, w/w)			Organic matter content (%)	Bulk density (Mg m^{-3})	Porosity (m^3 m^{-3})	Specific heat ±SD (J kg^{-1} K^{-1})
	1-0.1	0.1-0.02	<0.02				
All	3	57	40	4.00	1.09	0.59	699.2±38.8
<0.25	3	61	36	3.38	1.18	0.55	746.1
0.25-0.5	4	52	44	4.61	0.98	0.64	737.2
0.5-1	4	53	43	4.37	0.89	0.66	716.0
1-3	3	55	42	4.55	0.94	0.65	654.9
3-5	5	52	43	4.37	0.83	0.69	671.6
5-10	3	53	44	4.13	0.84	0.68	669.4
Aggregate size (mm) distribution (%)							
<0.25	0.25-0.5	0.5-1	1-3	3-5	5-10	>10	
17	17	16	17	15	10	8	

*Data from Sikora (1983), Witkowska-Walczak (2000), SD – standard deviation.

2.5.2. Field soils

The data used for the calculations of heat capacity come from Podlasie (Trzebieszów, 51°59′09.8”N 22°33′58.0”E). The Podzol soil (WRB, 2015)-contained 73.8%, 24.6, and 1.6% of sand (2-0.05 mm), silt (0.05-0.002 mm), and clay (<0.002 mm), respectively, and 69.5% of quartz (Usowicz *et al.*, 2009). The soil is further referred to as Polish sandy soil. Sandy soils are defined as soils that have a sand content greater than 50% and a clay content less than 20% (Huang and Hartemink, 2020). The biochar was obtained from wood chips at a pyrolysis temperature of 350-400°C and had a particle density of 1.41 g cm^{-3} and a bulk density of 0.328 g cm^{-3}. The specific heat of biochar is about 1.7 kJ kg^{-1} K^{-1}. Dry biochar (< 0.5-5 mm) was evenly distributed on the surface of 50 m^2 (5×10 m) plots in the amount of 0 (CK), 10 (B10), 20 (B20), and 40 (B40) Mg ha^{-1} and then mixed with the soil to a depth of 0-15 cm using a rototiller. The Decagon KD2 Pro meter was used to measure thermal conductivity, heat capacity, and thermal diffusivity.

The soil in Huantai (36°5′N, 117°58′E) is a Fluvic Cambisol according to the USDA classification (Soil Survey Staff, 1975) containing 70.8, 26.9, and 2.3% sand (2-0.05 mm), silt (0.05-0.002 mm), and clay (<0.002 mm) fractions, respectively (Table 2) (Zhang *et al.*, 2013; Zhao *et al.*, 2016). The soil is further referred to as Chinese sandy soil. The quartz content was assumed to be equal to the sand content (Zhang *et al.*, 2013). Black biochar powder at 4.5 and 9 Mg ha^{-1} was added to the soil in a random block pattern with a plot area of 36 m^2. The biochar was thoroughly mixed to a depth of 15 cm using rotary tillage. The biochar was obtained from the combustion of corncobs at 360°C and had a particle density of 1.80 g cm^{-3} and a bulk density of 0.30 g cm^{-3} (Zhao *et al.*, 2016). From the bulk density and water content (Fig. 1, Zhao *et al.*, 2016), and additionally from the particle density of soil and biochar, the volumetric contents of individual soil components were calculated. The contents were used to describe the probabilities of finding a given soil component in a single sample (Table 2). The volumetric contents and specific heat capacity of individual soil components were used in the statistical-physical model. The specific heat of biochar is 1.554 kJ kg^{-1} K^{-1}, and the average specific heat of organic matter and minerals is 0.725 kJ kg^{-1} K^{-1} (Zhao *et al.*, 2016). The heat pulse method was used to measure soil heat capacity and thermal diffusivity (Zhao *et al.*, 2016). Similarly, calculations were performed for the thermal conductivity of quartz content in sand, reducing the sand content by 10 and 20% and increasing the content of other minerals by 10% and 20% in silt (Usowicz *et al.*, 2020). Measured soil heat capacity data used in model validation were taken from the articles by Sikora (1983), Zhang *et al.* (2013), Zhao *et al.* (2016), and Usowicz *et al.* (2020).

Table 2. Measurement data of soil texture and organic matter content together with biochar of the control soil without biochar (CK) and soil amended with biochar at the level of 4.5 Mg ha^{-1} y^{-1} (B4.5) and 9.0 Mg ha^{-1} y^{-1} (B9.0) for the Chinese experimental field*

Soil+Biochar (Mg ha^{-1})	Sand	Silt	Clay	Organic matter
	(%)			
CK	70.8	26.9	2.3	1.5
B4.5	70.8	26.9	2.3	1.76
B9.0	70.8	26.9	2.3	2.02
with reduced sand by 10%				
CK	60.8	36.9	2.3	1.5
B4.5	60.8	36.9	2.3	1.76
B9.0	60.8	36.9	2.3	2.02
with reduced sand by 20%				
CK	50.8	46.9	2.3	1.5
B4.5	50.8	46.9	2.3	1.76
B9.0	50.8	46.9	2.3	2.02

*Data from Zhang *et al*. (2013) and Zhao *et al*. (2016).

The measurements of heat capacity in the Polish and Chinese experiments were conducted over a wide range of water contents, which varied significantly during the growing season due to rainfall and irrigation. In Poland, additional measurements were done in the laboratory at dry and saturated states.

2.5.3. Statistical evaluation

The agreement of the measured and modelled data was determined by mean squared error (*RMSE*) and maximum relative error (*MRE*):

$$RMSE = \sqrt{\frac{\sum_{i=1}^{n}(f_{mi}-f_{ci})^2}{k}}, \tag{30}$$

where f_{mi} is the measured value, f_{ci} is the calculated value, $k = n - 1$ if $n < 30$ and $k = n$ if $n > 30$, n is the number of data. The maximum relative error (*MRE*) was calculated from the equation:

$$MRE = \max_{i=1,2,\cdots,n}\left\{\left|\frac{f_{mi}-f_{ci}}{f_{mi}}\right| 100\%\right\}. \tag{31}$$

3. RESULTS

3.1. Soil aggregate beds

The specific heats of soil aggregates ranged from 654.9 for aggregates 1-3 mm to 746.1 J kg^{-1} K^{-1} for aggregates <0.25 mm. The specific heat was 737.2 and 716.0 for aggregates 0.25-0.5 and 0.5-1.0 mm and 671.6 and 669.4 J kg^{-1} K^{-1} for aggregates 3-5 and 5-10 mm (Table 1). The average specific heat for all aggregates in J kg^{-1} K^{-1} was 699.2 with a standard deviation of ±38.8. The measured and statistical-physical model predicted volumetric heat capacity (C_v) increased with the increasing water content and with the decreasing aggregate size (Fig. 3a, Table 1). The average

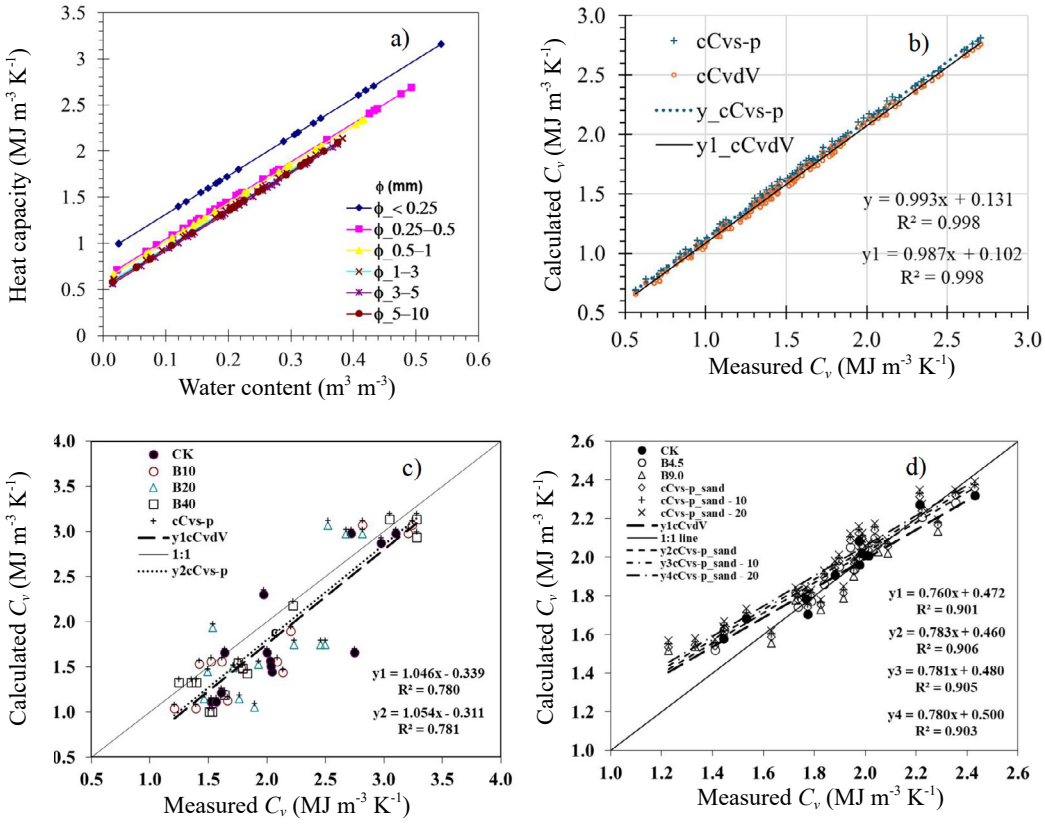

Fig. 3. Measured and calculated (c) heat capacities (Cv) from the statistical-physical (s-p) and de Vries (dV) models at various soil water contents. Measured heat capacities (Sikora, 1983) of various soil aggregates depending on the water content in the soil (a), comparison of measured and calculated heat capacities for various soil aggregates (b), comparison of measured (Usowicz *et al*., 2020) and calculated heat capacities in the field soil from Poland for different biochar additions: 0 (CK), 10 (B10), 20 (B20), and 40 (B40) Mg ha^{-1} (c), comparison of measured (Zhang *et al*., 2013; Zhao *et al*., 2016) and calculated heat capacities in the field soil from China for different biochar additions: 0 (CK), 4.5 (B 4.50), and 9.0 (B9.0); sand corresponds to the original sand content 70.8% and sand-10 and sand-20 are sand contents reduced by 10 and 20%, respectively (d).

values over the entire water content range recorded for the smallest aggregate fraction <0.25 mm was 1.886 MJ m^{-3} K^{-1}; it decreased consecutively for aggregates 0.25-0.5, 0.5-1, 1-3, 3-5, and 3-10 mm to 1.614, 1.468, 1.396, 1.352, and 1.339 MJ m^{-3} K^{-1}, respectively. The average C_v for all aggregate beds was 1.490 MJ m^{-3} K^{-1}, with a coefficient of variation CV (35.1%). The CV had the lowest value for fraction < 0.25 mm (29.53%) and the highest value for fraction 0.25-0.05 mm (36.56%). The statistical-physical model predicted means were higher by 0.12 MJ m^{-3} K^{-1} and those from the de Vries model were higher by 0.082 MJ m^{-3} K^{-1} than the measured mean of 1.490 MJ m^{-3} K^{-1} (Table 3). The minimum difference between the statistical-physical model-predicted and measured heat capacities was 0.09 (0.088) MJ m^{-3} K^{-1} for aggregates 0.25-0.05 mm (1.703 *vs*. 1.614), and the maximum was 0.157 MJ m^{-3} K^{-1} for aggregates 1-3 mm (1.553 *vs*. 1.396 MJ m^{-3} K^{-1}).

Depending on the aggregate size, the coefficients of variation (CV) for the model-predicted heat capacities were lower by 1.56 to 3.49% compared to those measured, varying from 29.5 to 34.8% (Table 3). The skewness values ranged from –0.332 to 0.269, indicating that the measured and model-predicted heat capacities were close to the normal distribution with a slight predominance of left-sided asymmetries. The kurtosis values ranged from –0.48 to –1.129, indicating that the distributions of the data sets tend to have a flat-topped curve.

The (linear) regression coefficient 'a' and determination coefficient R^2, *RMSE*, and *MRE* between the measured and predicted heat capacities for all aggregate fractions within <0.25-10 mm were 0.993, 0.998, 0.122 MJ m^{-3} K^{-1}, and 24.9%, respectively, for the statistical-physical model, and 0.987, 0.998 0.085 MJ m^{-3} K^{-1}, and 19.3%, for the de Vries model (Fig. 3b, and Table 3). In the case of the statistical-physical model, the regression coefficient 'a' and the coefficient of determination (R²) for each of the six aggregate fractions were also high and the same, *i.e*., 1.001 and 1, respectively. The root mean square errors (*RMSE*) ranged from 0.090 to 0.157 MJ m^{-3} K^{-1}, and the maximum relative error (*MRE*) was in the range from 10.7 to 24.9%. The regression coefficient 'a' close to unity, and the intercept of 0.131 in the regression equation between the heat capacities

Table 3. Root mean square error (*RMSE*) and maximum relative error (*MRE*) between the measured (m) heat capacity (C_v) and calculated by the statistical-physical (s-p) and de Vries (dV) models (c) for variously sized aggregate beds, linear regression coefficients 'a', intercepts, determination coefficients R^2, and basic statistics of measured and calculated heat capacities (SD – standard deviation, CV – coefficient of variation)

RMSE and *MRE* between measured and calculated values								
C_v	mCv_ cCvs-p	mCv_ cCvdV	mCv_ cCvs-p	mCv_ cCvs-p	mCv_ cCvs-p	mCv_ cCvs-p	mCv_ cCvs-p	mCv_ cCvs-p
Number of samples	n=467	n=467	n=63	n=78	n=70	n=80	n=90	n=86
Aggregate size (mm)	<0.25-10	<0.25-10	<0.25	0.25-0.5	0.5-1	1-3	3-5	5-10
RMSE (MJ m^{-3} K^{-1})	0.122	0.085	0.106	0.090	0.107	0.157	0.124	0.129
MRE (%)	24.9	19.3	10.7	12.2	15.5	24.9	21.7	22.6
Regression coefficient 'a'	0.993	0.987	1.001	1.001	1.001	1.001	1.001	1.001
Intercept	0.131	0.102	0.106	0.088	0.106	0.156	0.122	0.127
R^2	0.998	0.998	1.0	1.0	1.0	1.0	1.0	1.0

Basic statistics for selected aggregate sizes							
C_v	mCv	cCvs-p	cCvdV	mCv	cCvs-p	mCv	cCvs-p
Number of samples	467	467	467	63	63	78	78
Aggregate size (mm)	<0.25-10	<0.25-10	<0.25-10	<0.25	<0.25	0.25-0.5	0.25-0.5
Mean	1.490	1.610	1.572	1.886	1.993	1.614	1.703
SD	0.523	0.520	0.517	0.557	0.557	0.590	0.591
CV (%)	35.10	32.27	32.87	29.53	27.96	36.56	34.66
Minimum	0.565	0.689	0.660	0.996	1.102	0.715	0.803
Maximum	2.705	2.812	2.761	2.705	2.812	2.692	2.782
Skewnesss	0.225	0.205	0.198	–0.172	–0.172	0.269	0.267
Kurtosis	–0.481	–0.524	–0.536	–1.129	–1.129	–0.961	–0.959

Heat capacity Cv	mCv	cCvs-p	mCv	cCvs-p	mCv	cCvs-p	mCv	cCvs-p
Number of samples	n=70	n=70	n=80	n=80	n=90	n=90	n=86	n=86
Aggregate size (mm)	0.5-1	0.5-1	1-3	1-3	3-5	3-5	5-10	5-10
Mean	1.468	1.575	1.396	1.553	1.352	1.476	1.339	1.468
SD	0.486	0.486	0.486	0.487	0.413	0.413	0.432	0.433
CV (%)	33.08	30.87	34.83	31.34	30.52	27.99	32.28	29.48
Minimum	0.680	0.785	0.627	0.783	0.566	0.689	0.565	0.692
Maximum	2.354	2.462	2.159	2.317	2.075	2.198	2.073	2.201
Skewnesss	0.079	0.075	–0.060	–0.060	–0.265	–0.265	–0.332	–0.332
Kurtosis	–0.832	–0.830	–1.020	–1.017	–0.552	–0.553	–0.842	–0.840

measured and calculated with the statistical-physical model suggests that there is only a slight overestimation (close to zero) of the calculated heat capacity in the soil. This overestimation could be, in part, a derivative of a small error (not greater than 8%) of specific heat measurement using the calorimetric method (Sikora, 1983), as the heat of wetting of soil samples at pre-moistening to double hygroscopic water content was neglected.

3.2. Field soils

The average measured heat capacity of the Polish sandy soil with biochar (2.060 MJ m^{-3} K^{-1}) was greater than that calculated from the statistical-physical model (1.861 MJ m^{-3} K^{-1}) and the de Vries model (1.816 MJ m^{-3} K^{-1}) (Table 4). The CV for predicted data by both models was approximately 10% larger than the measured value (29.4%). The kurtosis value (–0.75) indicates that the distributions for the measured and calculated heat capacities were flattened. The skewness values indicate that the distribution of both the measured (0.68) and model-predicted data (0.87) had positive asymmetry. The regression coefficient 'a', R^2, *RMSE*, and *MRE* between the model-predicted heat capacities and measured were 1.054, 0.781, 0.391 MJ m^{-3} K^{-1}, and 42.1% for the statistical-physical model and 1.046, 0.781, 0.414 MJ m^{-3} K^{-1}, 44.4% for the de Vries model, respectively (Fig. 3c and Table 4).

For the Chinese sandy soil with biochar from China, the average measured heat capacity (1.868 MJ m^{-3} K^{-1}) was lower by 0.024 MJ m^{-3} K^{-1} than that calculated from the de Vries model and larger by 0.089 MJ m^{-3} K^{-1} (1.957 MJ m^{-3} K^{-1}) than the value obtained in the statistical-physical model (Table 4). The CV of the measured data set (15.5%) was larger than that of the model-predicted data (12.4%). The skewness indicates that the distribution of the measured heat capacities (–0.329) was left-tailed and the distribution of the model-predicted data was close to the normal distribution (skewness = 0.019). The distributions of the measured and calculated heat capacities were slightly flattened (kurtosis from –0.088 to –0.89). The statistical parameters, including the mean values and their variation spreads of the measured and computed distributions, accurately reflect the nature of the heat capacity distribution, while remaining reliable. The comparison of the heat capacities of the Chinese soil from the statistical-physical

Table 4. Root mean square error (*RMSE*) and maximum relative error (*MRE*) between the measured (m) heat capacity (C_v) and calculated by the statistical-physical (s-p) and de Vries (dV) models (c) for Polish and Chinese sandy soils, linear regression coefficients 'a', intercepts, determination coefficients R^2, and basic statistics of measured and calculated heat capacities (SD – standard deviation, CV – coefficient of variation, sand-10 – with reduced sand content by 10%, sand-20 – with reduced sand content by 20%

RMSE and *MRE* between measured and calculated values						
Cv	mCv_cCvs-p	mCv_cCvdV	cCvs-p	cCvs-p_sand-10	cCvsp_sand-20	cCvdV
Number of samples	53	53	33	33	33	33
Soils	Polish sandy soil + biochar			Chinese sandy soil + biochar		
RMSE (MJ $m^{-3}K^{-1}$)	0.391	0.414	0.109	0.119	0.130	0.102
MRE (%)	42.1	44.4	25.0	26.5	28.0	23.5
'a'	1.054	1.046	0.783	0.781	0.780	0.760
Intercept	–0.311	–0.339	0.460	0.480	0.500	0.472
R^2	0.781	0.781	0.906	0.905	0.903	0.901

Basic statistics								
Cv	mCv	cCvs-p	cCvdV	mCv	cCvs	cCvs-p_sand-10	cCvs-p_sand-20	cCvdV
Nr of samples	53	53	53	33	33	33	33	33
Soil	Polish sandy soil + biochar			Chinese sandy soil + biochar				
Mean	2.060	1.861	1.816	1.868	1.922	1.939	1.957	1.892
SD	0.605	0.722	0.717	0.289	0.238	0.238	0.237	0.232
CV (%)	29.38	38.81	39.47	15.49	12.38	12.25	12.13	12.24
Minimum	1.210	1.039	1.000	1.228	1.535	1.553	1.571	1.516
Maximum	3.281	3.195	3.136	2.430	2.357	2.376	2.395	2.320
Skewnesss	0.682	0.870	0.865	–0.329	0.002	0.004	0.005	0.019
Kurtosis	–0.731	–0.755	–0.754	–0.088	–0.892	–0.891	–0.890	–0.889

model and measured values (Zhao *et al.*, 2016) for different sand contents showed that the regression coefficient 'a', R^2, RMSE, and MRE were 0.780-0.783, 0.901-0.906, 0.109-0.130 MJ m^{-3} K^{-1}, and 25.0-28.0% and were similar to the de Vries model, namely 0.760, 0.901, 0.102 MJ m^{-3} K^{-1}, and 23.5%, respectively (Fig. 3d and Table 4). It is worth noting that the same statistical parameters were good and comparable, *i.e.*, 0.748, 0.919, 0.097 MJ m^{-3} K^{-1}, and 21.6% between the measured and predicted heat capacities when the analytic Zhao *et al.* (2016) model was used for the same original data as in this study.

The comparison of the statistical parameters indicates that the predictability of heat capacity by both the statistical-physical and de Vries models was better for soil aggregates than for field soils.

4. DISCUSSION

The novel model presented in this work, based on the concepts of specific heat, the principle of conservation of energy, and all configurations of mineral, organic, water, and air particles, demonstrates good accuracy in predicting soil volumetric heat capacity. The good agreement between the model-predicted and measured heat capacity, as indicated by the statistical parameters, confirms that the model assumptions regarding the specific heats of soil components (in kJ kg^{-1} K^{-1}: 0.733 for quartz at 20°C, 0.860 for other minerals, 1.92 for organic matter, and 1.554 for biochar) taking into account their change with changes in temperature, pressure, and density were adequately established. The model-predicted heat capacity allowed separating beds with different aggregate sizes and indicated the differences between soil types using field soils.

4.1. Soil aggregate beds

The increasing heat capacity with the decreasing aggregate size (from 10 to <0.25 mm) in aggregate beds predicted by the statistical-physical model can be attributed to the greater bulk density (Table 1) and the related higher volumetric fraction of soil solids composed of mineral and organic matter (Nimmo, 2004). This explanation can be supported by the results, which indicate that the soil heat capacity is positively correlated with the amount of mineral components and organic matter content, as well as the associated water content, including tightly bound water on clay surfaces and organic matter, even after drying at 105°C (*e.g.*, Wang *et al.*, 2019). This implies that the observed results can be suitable for analysing soil heat capacity changes under different land uses and other management practices that significantly affect aggregate size distribution and bulk densities (Nimmo, 2004). Dynamic changes in these variables occur under field conditions in recently disturbed soil due to soil subsidence and rainfall. A slight impact of organic matter is expected due to the similar contents of organic matter in all the aggregate fractions from 3.38 to 4.55% (Table 1). It is worth noting that larger versus smaller soil structural units (1-10 *vs*. <0.25 mm) provide the most suitable soil physical conditions for plant establishment and growth (Tisdal and Oades, 1982; Dilkova *et al.*, 2002). Suitable plant growth conditions in 1-10 mm aggregates are attributed to high water-holding capacity, moderate saturated hydraulic conductivity, and sufficient aeration (Tisdal and Oades, 1982; Gliński and Lipiec, 2018). Our results suggest that lower heat capacity can be an additional physical factor contributing to suitable plant growth conditions in 1-10 mm aggregates. This issue needs further study.

Furthermore, the alterations in heat capacity between different aggregate soil structures observed in this study provide new quantitative data for improved calculation of soil heat flux density (Wang and Bou-Zeid, 2012; Zheng *et al.*, 2015) in variously structured soils. Depending on the aggregate structure, the measured volumetric heat capacity in our study varied from 1.339 to 1.886 MJ m^{-3} K^{-1}, while its constant values are often used for calculating heat flux density in soil, *e.g.* 1.26 MJ m^{-3} K^{-1} (Wang and Bou-Zeid, 2012) or 2.0 MJ m^{-3} K^{-1} (Zheng *et al.*, 2015). Although the above results are based on a large number of replicates (467), they come from one soil type (Haplic Phaeozem) with relatively high organic matter. Therefore, further studies are needed for other soil types to perform more robust and reliable checks.

The analysis of the statistical parameters indicates that the agreement between the measured and calculated heat capacities was generally better for soil aggregates than for field soils (Tables 2 and 3). This can be demonstrated by the higher coefficients of determination (R^2), which indicate the degree to which the observed results are replicated by the model for soil aggregates (0.998) compared to field soils (0.781-0.906). This could be due to the use of the calorimetric method for measuring the heat capacity in soil aggregate beds and the heat pulse method with field soils. Research has demonstrated that heat capacities measured by the heat pulse method, compared to those calculated by models, show a characteristic trend of heat capacities to be lower at lower water contents, unchanged at medium water contents, and higher at higher water contents (Gnatowski *et al.*, 2022; Zhang *et al.*, 2013; Zhao *et al.*, 2016; Usowicz *et al.*, 2020). The differences in unsaturated soil can be attributed poor thermal contact between the probe and soil particles due to air-filled pores, creating a temperature discontinuity and artificial thermal lag (He *et al.*, 2018). Another reason for the discrepancies between the measured and calculated heat capacities at small scale can be the size and geometry of the heater and response elements, which measure the temperature in the pulse heat method (Gnatowski *et al.*, 2022). The question arises as to the extent to which measurements using the heat pulse method are reliable in the entire range of water content. On the other hand, heat capacities measured with the calorimetric method and calculated from the models show

a tendency to slightly overestimate the calculated ones over the entire range of water content. To improve the accuracy and extend the suitability of the heat pulse method in heterogeneous soils, *in-situ* probe spacing calibration (Zhang *et al.*, 2020) and the iterative local updating ensemble smoother (ILUES) algorithm for data assimilation (Xie *et al.*, 2025) were proposed. Further comparisons of measured and computed heat capacities from different models, as well as a more accurate understanding of heat energy transfer processes in the measurement methods used, can contribute to improving the accuracy of measured heat capacities of soils. Another cause of the weaker agreement between the measured and calculated heat capacity in field soils compared to aggregate beds can be the greater spatial variability of thermal properties in the former.

4.2. Field soils

The variation range in the heat capacity between the Polish and Chinese sandy soils was much less than that for variously sized aggregates of the Haplic Phaeozem. The similar values of the volumetric heat capacity in both sandy soils may be a consequence of the comparable contents of sand (quartz) from 70.8 to 73.8%, which typically affect soil heat capacity (Wang *et al.*, 2019). The essential effect of the quartz sand can be supported by the greater mean heat capacities (over the water content range) predicted by the statistical-physical model in both Polish and Chinese sandy soils (1.861-1.957 MJ m^{-3} K^{-1}) than in the aggregate beds of the fine-textured Polish soil with lower sandy quartz content (1.490 MJ m^{-3} K^{-1}). Some differences between the model-predicted and measured soils in particular, were likely a result of the different spatial distribution of the thermal properties in the experimental fields. The statistical parameters indicated that the performance of the novel model exhibited slightly better accuracy than that of the traditional analytic de Vries model that relies on the volume fractions of heat capacities of separate soil components (de Vries, 1963).

4.3. Suitability of the novel model and heat capacity data

An advantage of the novel statistical-physical heat capacity model is that it does not require the selection of parameters in the equations by comparing measured values with those calculated from equations independent of the porous medium, unlike existing models, such as those by de Vries (1963) and Zhao *et al.* (2016). However, the proposed model requires knowledge of the specific heat capacity of a medium composed of two or more components. For example, in the case of a medium composed of air and water, the model initially achieves the heat capacity of air, which fills the entire volume, and changes as the water content increases until it reaches the heat capacity of water. This is a result of model scaling, which is determined by the same equivalent radius of spheres, $r_k = 0.08$, assumed for each component of the medium. This makes the statistical-physical heat capacity model universal because it can calculate the heat capacities not only of soil but also of other porous media.

The data on soil heat capacity affecting heat storage (Wang *et al.*, 2019; Gnatowski *et al.*, 2022) along with thermal conductivity and thermal diffusivity impacting heat transfer through the soil (Usowicz *et al.*, 2013, 2020) are valuable across many fields, including evaluating how a soil warms or cools due to exchanges of energy through conduction, convection, and radiation, depending on soil structure. It is worth adding that numerous soil management practices, including tillage, land use, and conditioners to modify soil structure, are available, *e.g.* in soil (Usowicz and Lipiec, 2022; Garbowski *et al.*, 2023). Accurate data on heat capacity can be useful for predicting heat transfer and freezing/melting in soil around heat exchangers and efficiency of pump systems under different soil structures (Tu *et al.*, 2017; Kodešová *et al.*, 2013; Zhou *et al.*, 2025).

5. CONCLUSIONS

This study developed a volumetric heat capacity model for soils based on the concepts of specific heat, the principle of energy conservation, and configurations of mineral, organic, water, and air particles. The model was evaluated using measured results from six soil aggregate beds (from <0.25 to 3-10 mm) and two sandy soils under field conditions at various water contents. The following conclusions can be drawn:

1. The novel model exhibited good (satisfactory) performance in estimating the volumetric heat capacity of variously sized aggregate beds and field soils. This confirmed that the model assumptions regarding the specific heats of the main soil components were adequately established.

2. The measured and statistical-physical model predicted volumetric heat capacities increased with the increasing water content and with the decreasing aggregate size.

3. The model's performance was better for soil aggregate beds than for the sandy soils. This can be attributed in part to the different methods used to measure heat capacity in both soil specimens and the greater variability in the latter.

4. The applicability of the statistical-physical model to evaluate heat capacity and heat transfer through the soil as affected by soil management and land use was discussed.

5. The results indicate that the performance of the novel model was similar to that of the existing de Vries (1963) and Zhao *et al*. (2016) models. Unlike these models, the novel model does not require the choice of parameters in the equations.

Author contributions: Bogusław Usowicz: conceptualization, investigation, software, writing – review and editing. Jerzy Lipiec: conceptualization, formal analysis, methodology, writing – original draft.

Conflicts of Interest: The authors declare that they have no known competing financial interests or personal relationships that could have appeared to influence the work reported in this paper.

Data availability. Data will be made available on request.

6. REFERENCES

Bi, J., Li, L., Liu, Z., Wu, Z., Wang, G., 2024a. Assessment and enhancement of soil freezing characteristic curve estimation models. Cold Reg. Sci. Technol. 218, 104090, https://doi.org/10.1016/j.coldregions.2023.104090

Bi, J., Pan, Y., Yang, S., Li, R., Wu, Z., 2024b. Predicting the volumetric heat capacity of freezing soils using the soil freezing characteristic curve. J. Hydrol. 645, 132151, https://doi.org/10.1016/j.jhydrol.2024.132151

Bi, J., Pan, Y., Yang, S., Zhao, G., Wu, Z., 2024c. A thermal conductivity model for granular geomaterials with low porosity during the freezing process. Int. J. Heat Mass Transf. 233 126050, https://doi.org/10.1016/j.ijheatmasstransfer.2024.126050

Bolinder, M.A., Crotty, F., Elsen, A., Frąc, M., Kismányoky, T., Lipiec, J., *et al*., 2020. The effect of crop residues, cover crops, manures and nitrogen fertilization on soil organic carbon changes in agroecosystems: A synthesis of reviews. Mitig. Adapt. Strateg. Glob. Change 25, 929-952, https://doi.org/10.1007/s11027-020-09916-3

Chun, B., Guldmann, J., 2018. Impact of greening on the urban heat island: seasonal variations and mitigation strategies. Comput. Environ. Urban Syst. 71, 165-176.

Clauser, C., 2021. Thermal storage and transport properties of rocks, I: Heat Capacity and Latent Heat. Encyclopedia of Solid Earth Geophysics. In: Gupta, H.K. (Ed.) Springer International Publishing 1760-1768, https://doi.org/10.1007/978-3-030-58631-7

COMSOL, Comsol application library. Phase Change Models, 2023, https://www.comsol.com/model/phase-change-474 (Retrieved January 16, 2025).

de Vries, D.A., 1963. Thermal properties of soils. In: van Wijk, W.R. (Ed.), Physics of Plant Environment, North-Holland Publishing Company, Amsterdam, 210-235.

Dilkova, R., Jokova, M., Kerchev, G., Kercheva, M., 2002 Aggregate stability as a soil quality criterion. Options Méditerranéennes A 50, 305-312.

Garbowski, T., Bar-Michalczyk, D., Charazińska, S., Beata Grabowska-Polanowska, B., Kowalczyk, A., Lochyński, P., 2023. An overview of natural soil amendments in agriculture. Soil Till. Res. 225, 105462, https://doi.org/10.1016/j.still.2022.105462

Gliński, J., Lipiec, J., 2018. Soil Physical Conditions and Plant Roots 1st Edition, CRC Press, 260, First Published 1990. Reissued 2018 by CRC Press Taylor and Francis Group.

Gnatowski, T., Ostrowska-Ligęza, E., Kechavarzi, C., Kurzawski, G., Szatyłowicz, J., 2022. Heat capacity of drained peat soils. Appl. Sci. 12, 1579, https://doi.org/10.3390/app12031579

Guidolotti, G., Zenone, T., Endreny, T., Pace, R., Ciolfi, M., Mattioni, M., *et al*., 2025. Impact of drought on cooling capacity and carbon sequestration in urban green area. Urban Climate 59, 102244, https://doi.org/10.1016/j.uclim.2024.102244

He, H., Dyck, M.F., Horton, R., Ren, T., Bristow, K.L., Lv, J., *et al*., 2018. Development and application of the heat pulse method for soil physical measurements. Rev. Geophys. 56, https://doi.org/10.1029/2017RG000584

Heitman, J.L., Basinger, J.M., Kluitenberg, G.J., Ham, J.M., Frank, J.M., Barnes, P.L., 2003. Field evaluation of the dual-probe heat-pulse method for measuring soil water content contribution. Vadose Zone J. 2(4), 552-560, https://doi.org/10.2113/2.4.552

Heitman, J.L., Horton, R., 2011. Coupled heat and water transfer in soil. In: Gliński, J., Horabik, J., Lipiec, J. (Eds), Encyclopedia of Agrophysics, Springer Dordrecht, Heidelberg, London, New York, 155-162.

Huang, J., Hartemink, A.E., 2020. Soil and environmental issues in sandy soils. Earth-Science Reviews, 208, 1-22. https://doi.org/10.1016/j.earscirev.2020.103295

Jiang, S., Dong, S., Ni, L., 2025. Performance of earth to air heat exchanger under freezing soil conditions, Appl. Therm. Eng. 262, 125269, https://doi.org/10.1016/j.applthermaleng.2024.125269

Kekelia, B., 2012. Heat transfer to and from a reversible thermosiphon placed in porous media. Ph.D. Thesis, The University of Utah, Salt Lake City, UT, USA, https://search.proquest.com/openview/d6b0c7ce0d1b891aa8a14e5d07d0e6a3/1?cbl=18750&diss=y&pq-origsite=gscholar (accessed on 21 September 2018).

Kluitenberg, G.J., 2002. Heat capacity and specific heat. In: Dane, J.H., Topp G.C. (Eds), Methods of soil analysis. Part 4. SSSA Book Ser. 5. SSSA and ASA, Madison, WI, 1201-1208.

Kodešová, R., Vlasáková, M., Fér, M., Teplá, D., Jakšík, O., Neuberger, P., Adamovský, R., 2013. Thermal properties of representative soils of the Czech Republic. Soil Water Res., 8, 141-150.

Lahoori, M., Jannota, Y., Rosin-Paumier, S., Boukelia, A., Masrouri, F., 2020. Measurement of the thermal properties of unsaturated compacted soil by the transfer function estimation method. Appl. Therm. Eng. 167, 114795. https://doi.org/10.1016/j.applthermaleng.2019.114795

Langa, S., Magwaza, L.S., Mditshwa, A., Tesfay, S.Z., 2024. Temperature effects on seed germination and seedling biochemical profile of Cannabis landraces. Int. J. Plant Biol. 15 1032-1053, https://doi.org/10.3390/ijpb15040073

Lei, H., Bo, Y., Ma, C., Wang, L., Zhang, W., 2023. Variation pattern and prediction model of clay specific heat capacity considering multi-factors. Rock and Soil Mechanics 44, Suppl. 1-11.

Li, Q., Feng, P., Wang, R., An, N., Bai, R., Yang, G., *et al*., 2025. Numerical simulation of frost heave and thaw settlement characteristics in a complex pipe-soil system in the seasonally frozen ground. Appl. Sci. 15, 4628, https://doi.org/10.3390/app15094628

Lipiec J., Walczak R., Witkowska-Walczak B., Nosalewicz A., Słowińska-Jurkiewicz A., Sławiński C., 2007. The effect of aggregate size on water retention and pore structure of silt loam soils of different genesis. Soil Till. Res. 97, 239-246.

Luo, Q., Guo, Y., Dai, A., Li, Y., Cheng, J., Wang, P., *et al.*, 2025. Research on the evaluation model of soil heat loss in solar greenhouses. Energy 322, 135665, https://doi.org/10.1016/j.energy.2025.135665

Nimmo, J.R., 2004. Aggregation: Physical Aspects. In: D. Hillel (Ed.), Encyclopedia of Soils in the Environment: London, Academic Press, 1-11.

Noborio, K., McInnes, K.J., Heilman, J.L., 1996. Measurements of soil water content, heat capacity, and thermal conductivity with a single TDR probe. Soil Sci. 161, 22-28.

Shehata, M., Heitman, J., Sayde, C., 2022. High-resolution field measurement of soil heat capacity and changes in soil moisture using a Dual-Probe Heat-Pulse Distributed Temperature Sensing approach. Water Resour. Res. 58, e2021WR031680, https://doi.org/10.1029/2021WR031680

Sikora, E., 1983. Thermal properties of aggregate soil samples for different aggregate diameter and moisture, Ph.D. Thesis, Agricultural University, Lublin, Poland, 106.

Sikora, E., Malicki, M., 1984. Determination of the specific heat of moist soil by a calorimetric method. Polish J. Soil Sci. 17, 1-2, 53-57.

Skauge, A., Fuller, N., Hepler, L.G., 1983. Specific heats of clay minerals: Sodium and calcium kaolinites, sodium and calcium montmorillonites, illite, and attapulgite, Thermochim. Acta 61, 139-145, https://doi.org/10.1016/0040-6031(83)80310-4

Soil Survey Staff, 1975. Soil Taxonomy: A Basic System of Soil Classification for Making and Interpreting Surveys. USDA-SCS Agriculture Handbook, U.S. Gov. Print. Office, Washington, D.C.

Tarnawski, V.R., Wagner, B., Leong, W.H., McCombie, M., Coppa, P., Bovesecchi, G., 2021. Soil thermal conductivity model by de Vries: Re-examination and validation analysis. Eur. J. Soil Sci. 72, 1940-1953. https://doi.org/10.1111/ejss.1311

Tisdall, J.M., Oades, J.M., 1982. Organic matter and water-stable aggregates in soils, J. Soil Sci. 33, 141-163, https://doi.org/10.1111/j.1365-2389.1982.tb01755.x

Tu, S., Zhang, X., Zhou, X., 2017. A revised thermal resistance and capacity model for the ground heat exchanger under freezing soil conditions and thermal performance analysis. Procedia Eng. 205, 19-26, https://doi.org/10.1016/j.proeng.2017.09.929

Usowicz, B., 2000. Statistical and physical models of mass and energy flow in a porous medium (in Polish). Acta Agrophys. 29, 3-113.

Usowicz, B., Lipiec J., 2022. Spatial variability of thermal properties in relation to the application of selected soil-improving cropping systems (SICS) on sandy soil, Int. Agrophys. 36, 269-284, https://doi.org/10.31545/intagr/152122

Usowicz, B., Lipiec, J., Łukowski, M., Bis, Z., Usowicz, J., Latawiec, A.E., 2020. Impact of biochar addition on soil thermal properties: Modelling approach. Geoderma 376, 114574, https://doi.org/10.1016/j.geoderma.2020.114574

Usowicz, B., Lipiec, J., Usowicz, J.B., Marczewski, W., 2013. Effects of aggregate size on soil thermal conductivity: comparison of measured and model-predicted data. Int. J. Heat Mass Transfer 57, 536-541.

Usowicz, B., Marczewski, W., Lipiec, J., Usowicz, J.B., Sokołowska, Z., Dąbkowska-Naskręt, H., *et al*., 2009. Water in the soil – ground and satellite measurements in studies on climate change (in Polish). Foundation for the Development of Agrophysical Sciences, Monograph, Lublin, Poland, 1-171, ISBN: 978-83-60489-14-7

Wang, Z.H., Bou-Zeid, E., 2012. A novel approach for the estimation of soil ground heat flux. Agric. For. Meteorol. 154-155, 214-221. https://doi.org/10.1016/j.agrformet.2011.12.001

Wang, H., Garg, A., Zhang, X., Xiao, Y., Mei, G., 2020. Utilization of coconut shell residual in green roof: hydraulic and thermal properties of expansive soil amended with biochar and fibre including theoretical model. Acta Geophysica 68, 1803-1819, https://doi.org/10.1007/s11600-020-00492-3

Wang, Y.J., Lu, Y.L., Horton, R., Ren, T.S., 2019. Specific heat capacity of soil solids: influences of clay content, organic matter, and tightly bound water. Soil Sci. Soc. Am. J. 83, 1062-1066, https://doi.org/10.2136/sssaj2018.11.0434

Wang, Y., Zhang, Z., Guo, Z., Chen, Y., Yang, J., Peng, X., 2023. In-situ measuring and predicting dynamics of soil bulk density in a non-rigid soil as affected by tillage practices: Effects of soil subsidence and shrinkage. Soil Till. Res. 234, 105818, https://doi.org/10.1016/j.still.2023.105818

Witkowska-Walczak, B., 2000. Aggregate structure of mineral soils *vs*. hydrophysical characteristics (model investigations) (in Polish). Acta Agrophys. 30, 1-94.

WRB IUSS Working Group, 2015. World reference base for soil resources 2014, update 2015. International Soil Classification System for Naming Soils and Creating Legends for Soil Maps. World Soil Resources Reports No. 106, FAO, Rome.

Xie, X., Zeng, L., Ren, T., 2025. A data assimilation-based heat pulse method for monitoring soil hydraulic and thermal parameters in root zones, Soil Till. Res. 254, 106738, https://doi.org/10.1016/j.still.2025.106738

Zhang, X., Han, Z., Li, X., 2024. Accurate identification of soil thermal parameters and groundwater flow from thermal response tests. Renew. Energy 236, 121393, https://doi.org/10.1016/j.renene.2024.121393

Zhang, M., Lu, Y., Ren, T., Horton, R., 2020. In-situ probe spacing calibration improves the heat pulse method for measuring soil heat capacity and water content. Soil Sci. Soc. Am. J. 84, 1620-1629, https://doi.org/10.1002/saj2.20124

Zhang, Q., Wang, Y., Wu, Y., Wang, Y., Du, X., Liu, Z., *et al*., 2013. Effects of biochar amendment on soil thermal conductivity, reflectance, and temperature. Soil Sci. Soc. Am. J. 77, 1478-1487.

Zhao, J., Ren, T., Zhang, Q., Du, Z., Wang, Y., 2016. Effects of biochar amendment on soil thermal properties in the North China Plain. Soil Sci. Soc. Am. J. 80, 1157-1166.

Zheng, D.H., van der Velde, R., Su, Z.B., Wang, X., Wen, J., Booij, M.J., *et al.*, 2015. Augmentations to the Noah model physics for application to the Yellow River source area. Part II: Turbulent heat fluxes and soil heat transport. J. Hydrometeorol. 16, 2677-2694, https://doi.org/10.1175/JHM-D-14-0199.1

Zhou, J., Wang, X., Xu, J., Shi, Z., 2025. Heat exchange efficiency and structural stability of assembled energy shafts: a novel shallow geothermal exploitation system for coastal urban cities. Geotherm. Energy 13, 25, https://doi.org/10.1186/s40517-025-00350-9

Zografos, A.I., Martin, W.A., Sunderland, J.E., 1987. Equations of properties as a function of temperature for seven fluids. Comput. Methods Appl. Mech. Eng. 61, 177-187.